Reversible Photoinduced Wettability Transition of Hierarchical ZnO Structures

ARTICLE *in* THE JOURNAL OF PHYSICAL CHEMISTRY C · JANUARY 2009

Impact Factor: 4.77 · DOI: 10.1021/jp8085057

Article

Reversible Photoinduced Wettability Transition of Hierarchical ZnO Structures

Evie L. Papadopoulou, Marios Barberoglou, Vassilia Zorba, Aleka Manousaki, Alexios Pagkozidis, Emmanuel Stratakis, and Costas Fotakis

J. Phys. Chem. C, **2009**, 113 (7), 2891-2895• Publication Date (Web): 23 January 2009

Reversible Photoinduced Wettability Transition of Hierarchical ZnO Structures

Evie L. Papadopoulou,[†] Marios Barberoglou,[†,‡] Vassilia Zorba,[†,||] Aleka Manousaki,[†] Alexios Pagkozidis,[†,§] Emmanuel Stratakis,*[,†,§] and Costas Fotakis[†,‡]

Institute of Electronic Structure & Laser, Foundation for Research & Technology—Hellas (IESL-FORTH), P.O. Box 1385, Heraklion 711 10, Greece, Physics Department, University of Crete, Heraklion 714 09, Greece, and Materials Science and Technology Department, University of Crete, Heraklion 710 03, Greece

Received: September 25, 2008; Revised Manuscript Received: December 5, 2008

Control over the wettability of solids as well as the manufacturing of functional surfaces with special wetting properties has aroused much interest because of great advantages given to various applications in daily life, industry, and agriculture. We report here the dynamic optical control of the wetting behavior of liquids on hierarchically structured ZnO surfaces produced by irradiating silicon (Si) wafers with femtosecond laser pulses and subsequently coating them with ZnO by pulsed laser deposition. The final surface exhibits roughness at two length scales, comprising micrometer-sized Si spikes decorated with ZnO nanoprotrusions. It is shown that a liquid droplet on these surfaces can be rapidly and reversibly switched between hydrophobicity and superhydrophilicity by alternating UV illumination and dark storage or thermal heating. By studying the magnitude and the rate of the photoinduced transitions, we investigated the contribution of roughness at different scales in the framework of two theoretical wettability models.

Introduction

During the past decade there has been an increasing interest in controlling the wettability of solids, which depends on the free energy and the geometry of the surface in question. For many applications, it would be highly advantageous to be able to dynamically manipulate the behavior of liquids on surfaces, including the contact angle, droplet mobility, and effective area of the solid−liquid interface.[1−4] Functional surfaces that can be reversibly switched between hydrophobicity and hydrophilicity under the action of external stimuli have aroused great interest due to a wide range of potential applications, including intelligent microfluidic and laboratory-on-chip devices, controllable drug delivery, and self-cleaning surfaces.[5−7] Control over surface geometry and chemistry are two approaches to tailor wettability and thus develop smart surfaces.[1,8,9]

Among other materials, the wetting properties of metal oxides, mainly of ZnO and TiO_2, have been widely studied, since their wettability can be reversibly switched between superhydrophobicity and superhydrophilicity by alternation of ultraviolet (UV) irradiation and dark storage.[10−12] In addition, recent studies have revealed that micro- and nanostructures exhibiting hierarchical roughness cause an amplification of photoresponsive contact angle switching.[8,13] So far, previous works have been focused mainly on ZnO nanorods, nanowires, and nanobelts.[10,14,15] However, the remaining big challenge is to develop simple and reliable synthetic methods for ZnO hierarchical architectures with controlled morphology, which are important for exploring in detail the effect of roughness on wetting response.

In the present study, a two-step approach is developed in order to obtain a ZnO surface exhibiting roughness at two length scales. Microscale roughness, in the shape of spikes, is achieved on a Si wafer by structuring with femtosecond laser pulses.[16] Nanoscale roughness is subsequently realized by coating the laser-structured surface with ZnO nanograins grown by pulsed laser deposition (PLD).[17] Consequently, an enhancement of the nanoscale roughness is realized, and the final ZnO surface comprises hierarchical microstructures and nanostructures. It was shown that UV light can induce superhydrophilicity in the hydrophobic structures, while the hydrophobic state can be restored by dark storage or low-temperature heating in air. A sharp photoinduced transition between two distinct wetting states occurs, and its relation to roughness has been explained in the context of the Cassie−Baxter (CB) and Wenzel theoretical models.[18,19] A comparison of the rough surfaces to a nanostructured thin film, prepared under the same experimental conditions, has also been realized.

Experimental Section

A two-step method was developed for the fabrication of ZnO nanostructures on Si spikes. The first step involved microstructuring of the flat silicon (Si) surface using an ultrafast laser under a reactive gas (SF_6) atmosphere. Single-crystal *n*-type Si (100) wafers with a resistivity of $\rho = 2-8\ \Omega$ cm were subjected to laser irradiation in a vacuum chamber evacuated to a residual pressure of 10^{-2} mbar. A constant SF_6 pressure of 500 Torr was maintained during the process through a precision microvalve system. The irradiating laser source was constituted by a regenerative amplified Ti:sapphire laser ($\lambda = 800$ nm) delivering 150 fs pulses at a repetition rate of 1 kHz. The sample was mounted on a high-precision *X-Y* translation stage normal to the incident laser beam. A mechanical shutter was synchronized to the translation stages, exposing each given spot on the Si surface to an average of 500 pulses. Two laser fluences were used for the Si structuring, namely 0.17 and 2.1 J/cm^2. After laser irradiation, the microstructured surfaces were first cleaned in ultrasonic baths of trichloroethylene, acetone, and methanol followed by a 10% HF aqueous treatment in order to remove

* To whom correspondence should be addressed. E-mail: stratak@iesl.forth.gr. Telephone: +30-2810391274. Fax: +30-2810391305.
[†] Foundation for Research & Technology.
[‡] Physics Department, University of Crete.
[§] Materials Science and Technology Department, University of Crete.
[||] Current address: Lawrence Berkeley National Laboratory, MS70-108B, 1 Cyclotron Rd., Berkeley, CA 94720.

10.1021/jp8085057 CCC: $40.75
Published on Web 01/23/2009

the oxide grown on the surface. In the second step, the freshly prepared Si-patterned surfaces were coated with ZnO, using the conventional PLD technique in a flowing oxygen environment. A KrF excimer laser (Lambda Physik, $\lambda = 248$ nm, $\tau = 34$ ns pulse duration, 600 mJ/pulse maximum) was used for the ablation of a ZnO target, delivering 2500 pulses at a repetition rate of 10 Hz. The beam was incident on a rotating target at an angle of 45° with respect to the target normal and was focused with a spherical lens to yield an energy fluence of 1.5 J/cm^2 per pulse. The base pressure prior to deposition was more than 10^{-6} mbar, while the partial oxygen pressure during deposition was kept constant at 5×10^{-2} mbar. The Si substrate was placed parallel to the target at a distance of 4 cm and heated to 650 °C using a resistive heater. The samples were cooled to room temperature in the same oxidized environment used during deposition. In this work, we have used three types of substrates, namely, sample A (the Si microstructure prepared at 0.17 J/cm^2), sample B (the Si microstructure prepared at 2.1 J/cm^2), and a nanostructured thin film.

The morphology of the samples' surfaces, prior as well as after the deposition of ZnO, was characterized by field emission scanning electron microscope (FE-SEM, JEOL 7000) equipped with an energy dispersive X-ray spectrometer (EDX). The latter was used for the study of the elemental composition of the samples. An image processing algorithm was implemented in order to obtain quantitative information concerning topological characteristics, i.e., spike density, height, cone tip radius, and distribution, of the formed structures from the top and side views of the FE-SEM pictures of the structured areas.

The crystalline structure of the ZnO films was determined by X-ray diffraction (XRD) measurements using a Rigaku D/MAX-2000H rotating anode (12 kW) Cu Kα monochromated diffractometer. The films were measured at $\theta/2\theta$ configuration.

Static contact angle (CA) measurements were performed by an automated tension meter, using the sessile drop method. The contact angle was found to remain the same, within experimental error, for droplets in the 1−5 μL volume range. A minor decrease of 3° was measured in the case of a 0.5 μL droplet. Therefore, a 2 μL distilled deionized millipore water droplet was gently positioned on the surface using a microsyringe, and images were captured to measure the angle formed at the liquid−solid interface. The contact angle hysteresis (CAH), defined as the difference between the advancing and receding angles, has also been measured. Light induced hydrophilicity was studied by irradiating the samples for certain time intervals using selective femtosecond-pulsed UV laser irradiation (248 nm), with an intensity of 14 mW cm^{-2}. A monochromatic pulsed laser source is a preferable alternative to conventional UV lamps in terms of photoconversion efficiency because the process can be significantly accelerated, while avoiding a wider spectral distribution that often includes unwanted visible wavelengths known to inhibit the photoinduced transition.[20] After each irradiation interval, a 2 μL water drop was placed on the irradiated area, and the corresponding contact angle was measured. Following irradiation, the samples were either stored in the dark at room temperature or annealed for 1 h at 200 °C under ambient conditions. Subsequently, the respective time-dependent contact angle variations were determined.

Results

Figure 1a shows FE-SEM pictures of the microstructured silicon surfaces. Laser irradiation creates a surface morphology comprising a highly uniform and densely packed array of micrometer-sized conical structures (spikes). At higher laser fluence, the spike aspect ratio increases, resulting in a significant enhancement of the overall roughness.[21] As we have previously reported,[21] femtosecond laser structuring at different fluences allows one to control the wetting properties of Si surfaces. The water contact angle increases with laser fluence from 65° (flat Si) to ∼129° for the surface prepared at 0.17 J/cm^2 and to ∼150° for the surface prepared at 2.1 J/cm^2.

Surface morphology of a ZnO thin film deposited on a flat Si substrate is presented in Figure 1b. It consists of nanosized grains of average diameter of approximately 50 nm, with a regular, hexagonal shape. The corresponding cross-sectional view depicts the columnar structure of the grains, suggesting that the film growth has a preferred orientation, perpendicular to the substrate plane. X-ray diffraction analysis confirmed that the as-deposited ZnO film is highly oriented along the (002) direction. Other orientations corresponding to (100) and (101) are present with very low relative intensities. In the as-deposited state, the ZnO film is hydrophilic, exhibiting a contact angle close to 80°.

Panels c and d of Figure 1 depict FE-SEM images of the morphology of samples A (Figure 3a) and B (Figure 3b), as acquired after the deposition of the nanograined ZnO film. As clearly seen, a significant enhancement of the nanoscale roughness is attained. The micrometer scale spikes have been decorated by nanosized protrusions, resulting in a hierarchically rough surface. The nanoscale features are more pronounced in sample A than those in sample B. The corresponding contact angle and CAH values were measured for sample A (CA = 120 ± 1° and CAH = 48 ± 2°) and for sample B (CA = 140 ± 1° and CAH = 37 ± 2°). The high CAH values denote that the droplet is strongly pinned to the surface; thus, the initial state of the droplet is stable.[22] Stoichiometry of the ZnO protrusions was confirmed by EDX measurements performed on different positions on the structured surfaces (Figure 1e). Elemental analysis of the EDX spectrum was found to be similar to that obtained in the flat part of the sample outside of the spiked area. In both cases, the ZnO coating was deposited under conditions identical to those used for the nanostructured thin film shown in Figure 1b.

Figure 2 depicts the contact angle evolution with UV irradiation time for the different ZnO structures employed. Both structured samples exhibit a significant photoinduced transition to superhydrophilicity, reaching a nearly zero contact angle in short time. More importantly, the contact angle reduction rate, being a measure of the efficiency of the light-induced process, is higher than that observed in other ZnO structures.[12,23] Counterintuitively, this rate is lower for sample B, which exhibits a higher total roughness (shown later). On the contrary, the nanostructured ZnO thin film shows a weak response to UV irradiation, as the wetting angle change in this case is much smaller for the same irradiation time.

It should be emphasized that the aforementioned wettability changes are reversible because both dark storage and thermal heating reconvert the superhydrophilic surfaces to their original states (Figure 3a). After UV irradiation, the samples were placed in the dark. Hydrophobicity for samples A and B was restored within 24 h, whereas the flat sample required 7 days storage in order to return to its initial wetting state (Figure 3b). Alternatively, thermal heating at 200 °C for 1 h can return all surfaces to their original hydrophobic state, speeding the reversibility process. All samples were subjected to numerous switching cycles (Figure 3c), without observing any deterioration of the irradiation efficiency or the reversibility behavior.

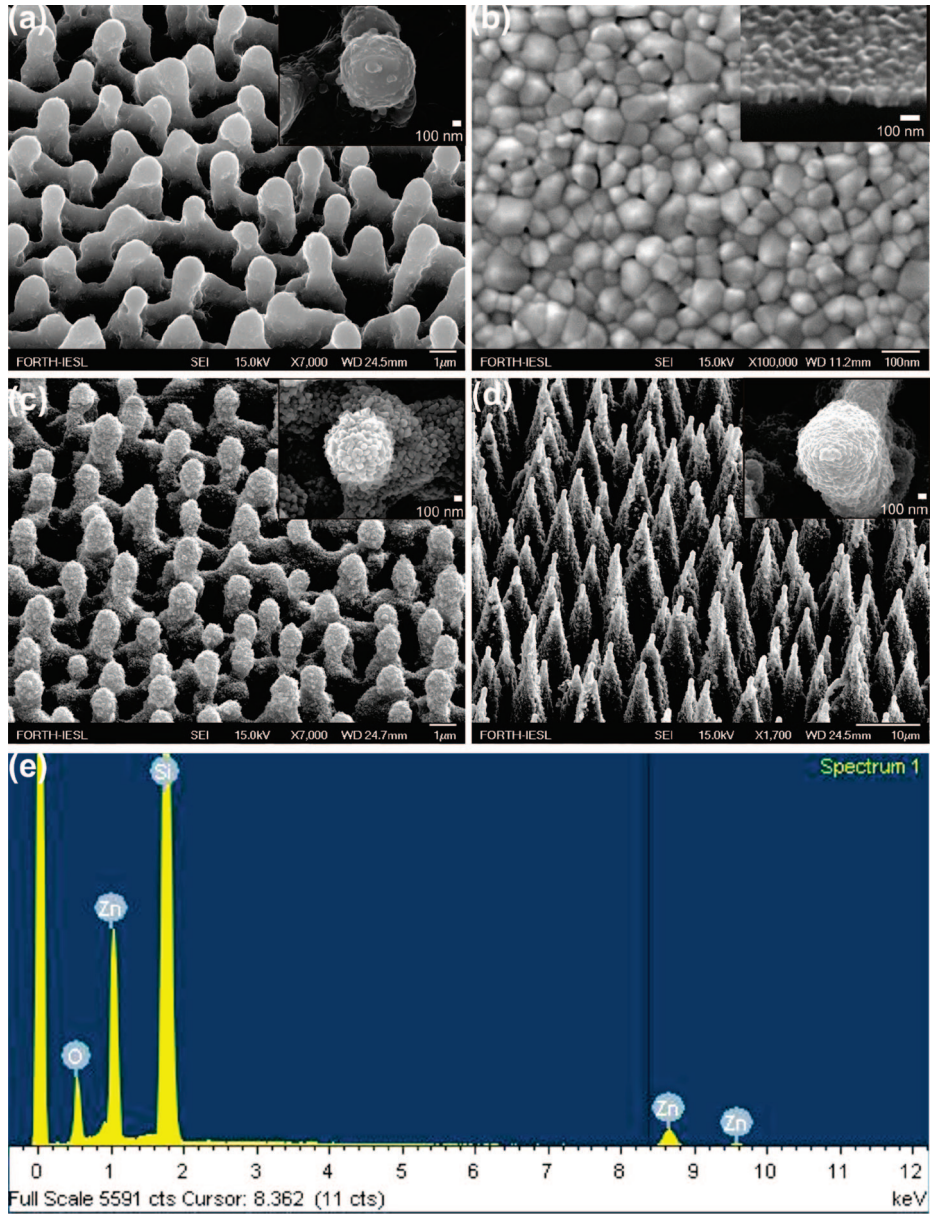

Figure 1. (a) Side SEM view of Si surfaces structured by femtosecond irradiation at a laser fluence of 0.17 J/cm^2. The inset shows a higher magnification of the top of a single microcone. (b) Top SEM view of a nanograined ZnO film prepared by PLD on a flat Si substrate. A cross-sectional image of the film is shown in the inset. (c) Side SEM view of a ZnO-coated Si surface structured by femtosecond irradiation at a laser fluence of 0.17 J/cm^2. Higher magnification of the top of a single microcone (scale bar is 100 nm), shown in the inset, reveals the double-scale roughness of the structures. (d) The same as in (c) but at a laser fluence of 2.1 J/cm^2. (e) Typical EDX spectrum from a ZnO-coated Si spike surface. Elemental analysis showed a 1.0:1.05 molar ratio of Zn:O_2.

Discussion

In order to understand the response of the as-deposited structures, one has to consider the effect of the macroscopic surface roughness on the wettability, which has been theoretically approached by two different models. In the Wenzel model,[19] the liquid is assumed to completely penetrate within the rough surface, and the apparent contact angle, θ_w, is given by

$$\cos \theta_w = r_w \cos \theta \qquad (1)$$

where r_w is the ratio of the actual over the projected surface area of the substrate and θ is the intrinsic contact angle on a flat surface of the same nature as the rough. Because r_w is always greater than unity, this model predicts that the contact angle of a liquid that wets a solid ($\theta < 90°$) decreases when its surface is roughened ($\theta_w < \theta$), while roughening a nonwetting flat surface ($\theta > 90°$) always increases its hydrophobicity ($\theta_w > \theta$). In contrast, Cassie and Baxter[18] assumed that the liquid does not completely permeate the roughened solid. As a result, air pockets are trapped inside the features underneath the liquid, which sits above a composite surface made of solid and air. In this case, the contact angle, θ_{CB}, is an average between the value on air (i.e., 180°) and the value on the flat solid (i.e., θ) and is given by

$$\cos \theta_{CB} = -1 + f(1 + \cos \theta) \qquad (2)$$

where f defines the fraction of the projected solid surface wetted by the liquid. As f is always lower than unity, this model always predicts enhancement of hydrophobicity, independent of the value of the initial contact angle θ. The lower the value of f, the smaller the solid−liquid contact area and the higher the increase in the measured contact angle. The effect of double-scale roughness on wettability has been recently addressed.[24−26]

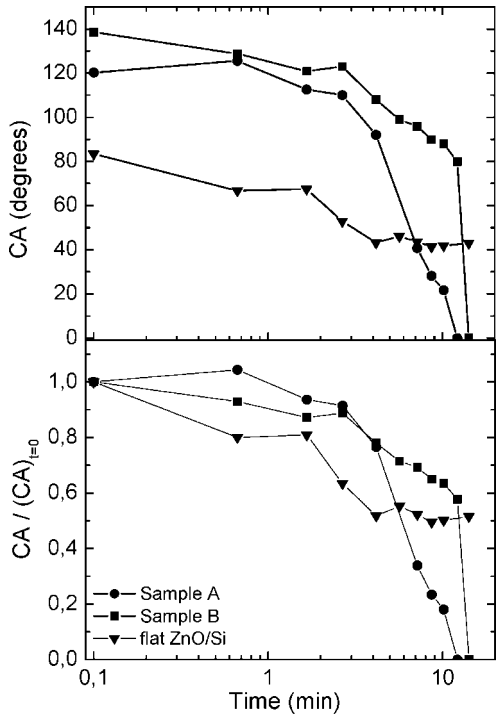

Figure 2. Dependence of the water contact angle on the UV illumination time for the flat and the structured ZnO samples studied. The corresponding evolution of the ratio of the respective contact angles to their initial values is also plotted for comparison.

Assuming that the two types of roughness are homothetic,[6] meaning that they occupy the same fraction of surface, f, the Cassie−Baxter equation is modified as follows

$$\cos\theta'_{CB} = -1 + f^2(1 + \cos\theta) \quad (3)$$

As $f < 1$, the comparison of eqs 2 and 3 shows that the contact angle of the dual roughness surface is always higher than in the single roughness case. There are many theoretical and experimental reports on the transition between the two basic wetting states described above under the action of various external stimuli.[27−30] However, to our knowledge, there are limited theoretical and no experimental reports for the effect of different roughness scales on the characteristics of this transition.

The initial contact angle of the flat ZnO sample is always lower than 90°, indicating that the as-deposited grains are hydrophilic. Following the results presented in Figure 2, it is obvious that the original contact angle values measured for the structured samples are consistent with the CB model because contrary to the Wenzel model, it predicts a rise in the wetting angle upon increasing the roughness of an initially hydrophilic ($\theta < 90°$) surface. Assuming that the intrinsic contact angle θ is measured on the flat film ($\theta = 83.4°$), eq 3 is used for the estimation of the f parameter for the two samples in their as-deposited state. The result is $f \sim 0.7$ for sample A and $f \sim 0.5$ for sample B. This means that sample B exhibits higher total roughness and, being in a Cassie−Baxter state, is less wetted by the water drop.

As also shown in Figure 2, in both samples the evolution of contact angles is gradual at short illumination times, followed by an abrupt change taking place at wetting angles lower than ~90°. This sharp transition toward superhydrophilicity suggests that the wetting state of the drop switches from the Cassie−Baxter state to the Wenzel state, as the latter is the model predicting the possibility of superhydrophilicity for very rough surfaces. The corresponding evolution of the composite roughness factor

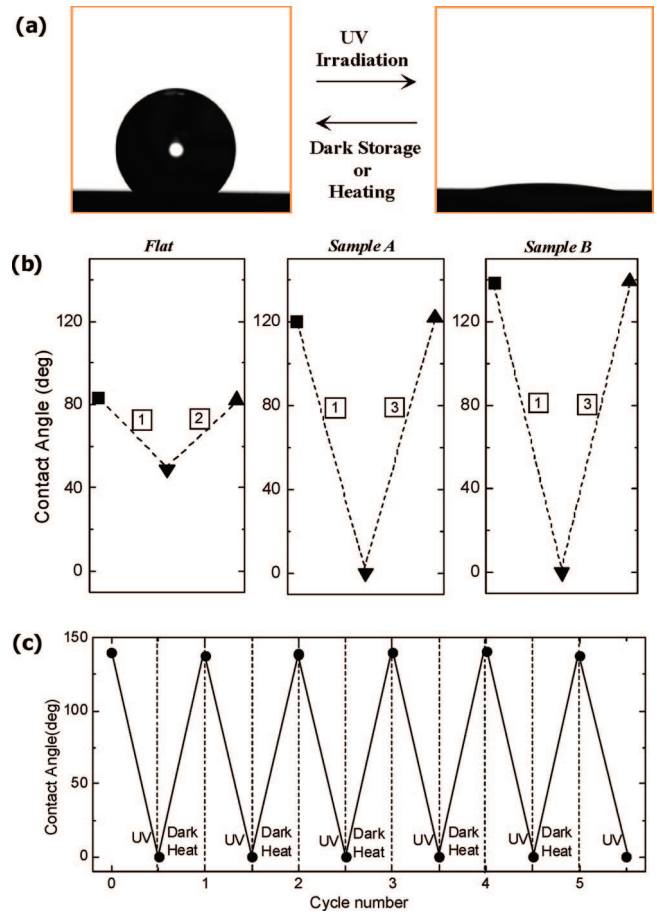

Figure 3. (a) Photographs of the shape of a water droplet on sample B before (left) and after (right) UV illumination. The transition from hydrophobicity to superhydrophilicity is reversible upon dark storage or thermal heating (Figure 3b,c). (b) Restoration of the UV light-induced wettability conversion upon sample storage in the dark. Processes 1, 2, and 3 denote UV illumination for 20 min and dark storage for 7 and 1 days, respectively. In all cases, the surface can be switched several times between the two states under the alternation of UV irradiation and dark storage. (c) Reversible switch from hydrophobicity to superhydrophilicity for sample B under the alternation of UV irradiation and thermal heating at 200 °C for 1 h. Sample A exhibits a similar response.

f up to the transition to the Wenzel state can be monitored using eq 3 and the contact angle values of Figure 2. This is plotted in Figure 4, where each point of the factor f had been obtained by substitution in eq 3 of the respective contact angle values for any given exposure time. As can be seen from this plot, the transition takes place when f equals values higher than unity, rendering the Cassie−Baxter model invalid.

It is known that UV irradiation generates electron−hole pairs[31] in the ZnO lattice.[8] Some of the holes react with lattice oxygen to form surface oxygen vacancies, while the electrons can react with the metal ions (Zn^{2+}) present in the lattice, forming Zn^{+} defective sites. Meanwhile, water and oxygen may compete to dissociatively adsorb on these vacancies. The Zn^{+} defective sites are kinetically more favorable for hydroxyl adsorption than oxygen adsorption. As a result, the surface hydrophilicity is improved, and the water contact angle is significantly reduced. It has also been demonstrated that the surface becomes energetically unstable after hydroxyl adsorption. Because oxygen adsorption is thermodynamically favored, it is more strongly bonded on the defect sites than on the hydroxyl groups.[23] Therefore, the hydroxyl groups adsorbed on the defective sites can be replaced gradually by oxygen atoms

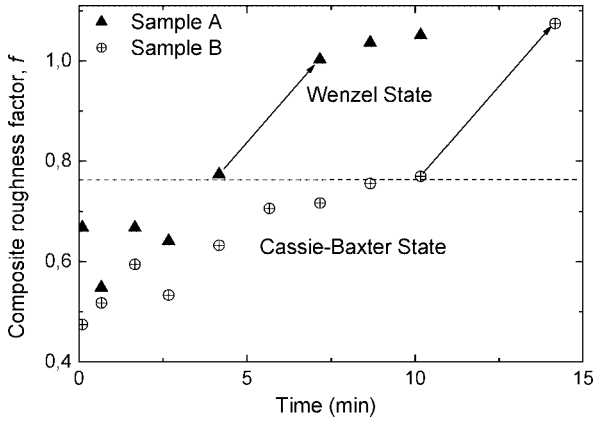

Figure 4. Dependence of composite roughness factor, *f*, on the UV irradiation time for samples A and B. Transition from the Cassie−Baxter to the Wenzel state occurs at a critical *f* denoted by the dashed line.

when the UV-irradiated samples are placed in the dark. Subsequently, the surface evolves back to its original state (before any UV irradiation), and the wettability is reconverted. Heat treatment accelerates the elimination of surface hydroxyl groups, and as a result, the hydrophilic surface converts quickly to a hydrophobic surface.[32] On the basis of the above analysis, it can be concluded that the reversible switching between hydrophobicity and superhydrophilicity is related to the synergy of the surface chemical composition and the surface roughness. The former provides a photosensitive surface, which can be switched between hydrophilicity and hydrophobicity, and the latter further enhances these properties.

As is shown in Figures 2 and 4, the final step to superhydrophilicity is more abrupt in the case of sample B where the microscale roughness is higher. This suggests that microscale roughness plays a major role in the transition from the Cassie−Baxter to the Wenzel state as it contributes more to the total roughness. In contrast, the transition to the Wenzel state occurs in shorter times for sample A, where the nanoscale roughness is more pronounced. This indicates that nanoscale roughness plays a more important role in the efficiency of the light-induced process. This may be attributed to the fact that the surface to volume ratio is higher in this case, and as a result, the total interface between water and the grown ZnO structures is high. This leads to an effective increase in photoactive defect sites, which are in contact with water molecules.

Conclusions

In conclusion, we have developed a two-step method to prepare ZnO structures showing hierarchical architectures combining microscale and nanoscale features. Such ZnO structures were found to exhibit a remarkable reversible transition to superhydrophilicity after exposure to UV light. We conclude that this technique can be employed to control the structural and morphological properties of ZnO structures, resulting in reversible efficient wettability changes. Such capability may be useful for self-cleaning coatings and microfluidic applications, as well as for studying the wettability of biological surfaces and its relation to microstructures and nanostructures.

Acknowledgment. This work was performed at the Ultraviolet Laser Facility operating at IESL-FORTH and is supported in part by the European Commission through the Research Infrastructures activity of FP6 (Laserlab-Europe RII3-CT-2003-506350). European project NATCO is acknowledged for the ZnO target.

References and Notes

(1) Feng, X.; Jiang, L. *Adv. Mater.* **2006**, *18*, 3063.
(2) Liu, Y.; Mu, L.; Liu, B.; Kong, J. *Chem.—Eur. J.* **2005**, *11*, 2622.
(3) Hayes, R. A.; Feenstra, B. J. *Nature* **2003**, *425*, 382.
(4) Ichimura, K.; Oh, S.-K.; Nakagawa, M. *Science* **2000**, *288*, 1624.
(5) Velev, O. D.; Prevo, B. G.; Bhatt, K. H. *Nature* **2003**, *426*, 515.
(6) Verplanck, N.; Coffinier, Y.; Thomy, V.; Boukherroub, R. *Nanoscale Res. Lett.* **2007**, *2*, 577.
(7) Zorba, V.; Stratakis, E.; Barberoglou, M.; Spanakis, E.; Tzanetakis, P.; Anastasiadis, S. H.; Fotakis, C. *Adv. Mater.* **2008**, *20*, 4049.
(8) Wang, S.; Song, Y.; Jiang, L. *J. Photochem. Photobiol., C* **2007**, *8*, 18.
(9) Barberoglou, M.; Zorba, V.; Anastasiadis, S. H.; Fotakis, C. *Appl. Surf. Sci.* 2008, available online, DOI: 10.1016/j.apsusc.2008.07.130.
(10) Feng, X.; Feng, L.; Jin, M.; Zhai, J.; Jiang, L.; Zhu, D. *J. Am. Chem. Soc.* **2004**, *126*, 62.
(11) Feng, X.; Zhai, J.; Jiang, L. *Angew. Chem., Int. Ed.* **2005**, *44*, 5115.
(12) Kenanakis, G.; Stratakis, E.; Vlachou, K.; Vernardou, D.; Koudoumas, E.; Katsarakis, N. *Appl. Surf. Sci.* **2008**, *254*, 5695.
(13) Rosario, R.; Gust, D.; Garcia, A. A.; Hayes, M.; Taraci, J. L.; Dailey, J. W.; Picraux, S. T. *J. Phys. Chem. B* **2004**, *108*, 12640.
(14) Badre, C.; Pauporte, T.; Turmine, M.; Lincot, D. *Nanotechnology* **2007**, *18*, 365705.
(15) Lao, C. S.; Li, Y.; Wong, C. P.; Wang, Z. L. *Nano Lett.* **2007**, *7*, 1323.
(16) Zorba, V.; Persano, L.; Pisignano, D.; Athanassiou, A.; Stratakis, E.; Cingolani, R.; Tzanetakis, P.; Fotakis, C. *Nanotechnology* **2006**, *17*, 3234.
(17) Papadopoulou, E. L.; Varda, M.; Kouroupis-Agalou, K.; Androulidaki, M.; Chikoidze, E.; Galtier, P.; Huyberechts, G.; Aperathitis, E. *Thin Solid Films* **2008**, *516*, 8141.
(18) Cassie, A. B. D.; Baxter, S. *Trans. Faraday Soc.* **1944**, *40*, 546.
(19) Wenzel, R. N. *Ind. Eng. Chem.* **1936**, *28*, 988.
(20) Rico, V.; Lopez, C.; Borras, A.; Espinos, J. P.; Gonzalez-Elipe, A. R. *Sol. Energy Mater. Sol. Cells* **2006**, *90*, 2944.
(21) Zorba, V.; Stratakis, E.; Barberoglou, M.; Spanakis, E.; Tzanetakis, P.; Fotakis, C. *Appl. Phys. A,* **2008**, *93*, 819.
(22) Nosonovsky, M.; Bhushan, B. *Microelectron. Eng.* **2007**, *84*, 382.
(23) Sun, R.; Nakajima, A.; Fujishima, A.; Wanatabe, T.; Hashimoto, K. *J. Phys. Chem. B* **2001**, *105*, 1984.
(24) Nosonovsky, M.; Bhushan, B. *Ultramicroscopy* **2007**, *107*, 969.
(25) Patankar, N. A. *Langmuir* **2004**, *20*, 8209.
(26) Shibuichi, S.; Onda, T.; Satoh, N.; Tsujii, K. *J. Phys. Chem.* **1996**, *100*, 19512.
(27) Lafuma, A.; Quere, D. *Nat. Mater.* **2003**, *2*, 457.
(28) Sbragaglia, M.; Peters, A. M.; Pirat, C.; Borkent, B. M.; Lammertink, R. G. H.; Wessling, M.; Lohse, D. *Phys. Rev. Lett.* **2007**, *99*, 15601.
(29) Bormashenko, E.; Pogreb, R.; Whyman, G.; Erlich, M. *Langmuir* **2007**, *23*, 6501.
(30) Dorrer, C.; Ruhe, J. *Langmuir* **2007**, *23*, 3820.
(31) Spanakis, E.; Stratakis, E.; Tzanetakis, P.; Fritzsche, H.; Guha, S.; Yang, J. *J. Non-Cryst. Solids* **2002**, *299−302*, 521.
(32) Miyauchi, M.; Kieda, N.; Hishita, S.; Mitsuhashi, T.; Nakajima, A.; Watanabe, T.; Hashimoto, K. *Surf. Sci.* **2002**, *511*, 401.

JP8085057